J Supercond Nov Magn (2016) 29:115–122
DOI 10.1007/s10948-015-3218-z

ORIGINAL PAPER

Lattice Strain and Magnetic Property Evolution of $La_{0.5}Sr_{0.5}Mn_{1-x}Co_xO_3$ Synthesized by Solid-State Reaction at Low Temperatures

Wen Chen[1] · Yuye Chen[1] · Wenwei Wu[1,2] · Tangwei Li[1] · Cuiyan Zhang[1] · Yuan Zhou[1] · Juan Wu[1]

Received: 30 June 2015 / Accepted: 12 September 2015 / Published online: 19 September 2015

Abstract $La_{0.5}Sr_{0.5}Mn_{1-x}Co_xO_3$ ($0 \leq x \leq 0.3$) is obtained by calcining the precursor carbonates in air. The precursor and its calcined products are characterized by X-ray powder diffraction, scanning electron microscopy, and vibrating sample magnetometer. A highly crystallized $La_{0.5}Sr_{0.5}Mn_{1-x}Co_xO_3$ ($0 \leq x \leq 0.3$) with a perovskite structure is obtained when the precursor is calcined at 900 °C in air for 3 h. The lattice strains of $La_{0.5}Sr_{0.5}Mn_{1-x}Co_xO_3$ increase with the increase of Co content and/or the decrease of Mn content between $x = 0$ and $x = 0.1$ at first, then decreases with the increase of Co content. The magnetic properties of $La_{0.5}Sr_{0.5}Mn_{1-x}Co_xO_3$ depend on the composition and measurement temperature. Cobalt substitution can markedly improve the coercivity of $La_{0.5}Sr_{0.5}Mn_{1-x}Co_xO_3$.

Keywords Manganites · Chemical synthesis · X-ray diffraction · Magnetic properties

1 Introduction

Perovskite-type oxides $Re_{1-x}A_xMnO_3$ (Re = La, Pr, Nd, Sm, etc. and A is an alkaline earth element or a divalent element such as Ca, Sr, Ba, or Pb) have recently attracted much attention due to their interesting properties, such as electrical, mechanical, optical, magnetic, and catalytic properties [1–12]. Thus, perovskite-type oxides have been widely used as electrode materials for solid oxide fuel cells [8, 12–14], chemical sensors [15, 16], oxygen-permeating membranes [17, 18], thermoelectric devices [19], catalysts [7, 20, 21], ferroelectrics, superconductors, and fluorescent materials [22]. Besides, perovskite-type oxide is also a promising magnetic refrigeration material [23–25]. Among the perovskite-type oxides, $La_{0.5}Sr_{0.5}MnO_3$ [26, 27] and doped $La_{0.5}Sr_{0.5}MnO_3$ [28–30] are important perovskite-type oxides. The structures and properties of these materials highly depend on the composition, synthesis method, and calcination temperature. Therefore, the properties of $La_{0.5}Sr_{0.5}MnO_3$ and its related materials can be regulated by the composition and synthesis method. Shi et al. [27] synthesized $La_{0.5}Sr_{0.5}MnO_3$ by conventional solid-state reaction at 1400 °C for 24 h using La_2O_3, $SrCO_3$, and MnO_2 powders as raw materials. Both the specific saturation magnetizations of the samples annealed in nitrogen and oxygen, respectively, are higher than those of the sample annealed in air. Xia et al. [28] prepared polycrystalline $La_{0.5}Sr_{0.5}Mn_{1-x}Ti_xO_3$ by a standard solid-state reaction method using La_2O_3, $SrCO_3$, MnO_2, and TiO_2 as raw materials. The results showed that $La_{0.5}Sr_{0.5}Mn_{1-x}Ti_xO_3$ sintered at 1573 K for 12 h suppresses the antiferromagnetic (AFM) charge ordering and leads to a step-like magnetization behavior below 3 K after doping Ti^{4+}. Yu et al. [30] synthesized $La_{0.7}Sr_{0.3}Mn_{1-x}Co_xO_3$ by conventional solid-state reaction using La_2O_3, $SrCO_3$, $MnCO_3$, and Co_2O_3 as precursors, followed by grinding, mixing, and calcination at 1200 °C for 24 h. The results showed that the ferromagnetic (FM)–paramagnetic (PM) phase transition temperature (T_C) values and magnetization

✉ Wenwei Wu
gxuwuwenwei@aliyun.com; wuwenwei@gxu.edu.cn

[1] School of Chemistry and Chemical Engineering, Guangxi University, Nanning 530004, People's Republic of China

[2] Guangxi Colleges and Universities Key Laboratory of Applied Chemistry Technology and Resource Development, Nanning 530004, People's Republic of China

decrease with the increase of Co concentration in the sample, attributed to the presence of Co ions (normally, with oxidation states 3+ and 4+ in manganites) which reduces FM interactions due to a decrease of the Mn^{3+}/Mn^{4+} ratio and to an enhancement of antiferromagnetic interactions between Co and Mn ions. Although many researchers have made great efforts to prepare $La_{1-x}Sr_xMnO_3$ and/or doped $La_{1-x}Sr_xMnO_3$, facile and scalable synthesis of $La_{1-x}Sr_xMnO_3$ and/or doped $La_{1-x}Sr_xMnO_3$ with high performance is still a significant challenge. Therefore, it is highly desirable and necessary to explore new synthesis methods and composition for the preparation of $La_{1-x}Sr_xMnO_3$ and/or doped $La_{1-x}Sr_xMnO_3$. To the best of our knowledge, the synthesis and magnetic properties of $La_{0.5}Sr_{0.5}Mn_{1-x}Co_xO_3$ by calcining precursor carbonates have rarely been reported in previous studies, due to the smaller ionic radii of Co^{3+} ion (0.061 nm) [31] and same unpaired electrons in 3d orbit compared to Mn^{3+} (0.064 nm) [32]. However, Co^{3+} ion (0.061 nm, d^6) has larger ionic radii and more unpaired electrons in 3d orbit than Mn^{4+} ion (0.053 nm, d^3) [33]; part of substitution of Mn^{3+} and/or Mn^{4+} ions by Co^{3+} ions in $La_{0.5}Sr_{0.5}MnO_3$ will lead to lattice strain and magnetic property changes.

This study aims to prepare $La_{0.5}Sr_{0.5}Mn_{1-x}Co_xO_3$ ($0. \leq x \leq 0.3$) by calcining carbonate in air and study the effect of composition and calcination temperature on structure, lattice strains, and magnetic properties of $La_{0.5}Sr_{0.5}Mn_{1-x}Co_xO_3$. Our results clearly show that the specific magnetizations of $La_{0.5}Sr_{0.5}Mn_{1-x}Co_xO_3$ decrease with the increase of Co concentration in the sample. However, the coercivity of $La_{0.5}Sr_{0.5}Mn_{1-x}Co_xO_3$ increases with the increase of Co concentration in the sample.

2 Experimental

2.1 Reagent and Apparatus

All chemicals used are of reagent-grade purity (purity >99.9 %). X-ray powder diffraction (XRD) was performed using an X'pert PRO diffractometer equipped with a graphite monochromator and a Cu target. The radiation applied was Cu Kα ($\lambda = 0.15406$ nm), operated at 40 kV and 50 mA. The XRD scans were conducted from 5 ° to 70 ° in 2θ, with a step size of 0.01 ° The morphologies of the synthesis products were observed using an S-3400 scanning electron microscope (SEM). The specific magnetizations (M) of the calcined sample powders were carried out at different measurement temperatures using a vibrating sample magnetometer (Lake Shore 7410).

2.2 Preparation of $La_{0.5}Sr_{0.5}Mn_{1-x}Co_xO_3$

The $La_{0.5}Sr_{0.5}Mn_{1-x}Co_xO_3$ precursor samples were synthesized by solid-state reaction at low temperatures [34, 35]. In a typical synthesis ($La_{0.5}Sr_{0.5}MnO_3$), La $(NO_3)_3{\cdot}6H_2O$ (15.00 g), $SrCl_2$ (5.49 g), $MnCl_2{\cdot}4H_2O$ (13.71 g), and Na_2CO_3 (19.85 g) were placed in a mortar, and the mixture was thoroughly ground by hand with a rubbing mallet for 40 min. The strength applied was moderate. The reactant mixture gradually became damp, and a paste was formed immediately. The reaction mixture was kept at 30 °C for 2 h. The mixture was washed with deionized water to remove soluble inorganic salts until SO_4^{2-} ion cannot be visually detected with a 0.5 mol L^{-1} $BaCl_2$ solution. The mixture was then washed with a small amount of anhydrous ethanol. $La_{0.5}Sr_{0.5}MnO_3$ precursor was obtained after being dried at 80 °C for 5 h. A similar synthesis procedure was used to synthesize other $La_{0.5}Sr_{0.5}Mn_{1-x}Co_xO_3$ precursor. Finally, perovskite-type $La_{0.5}Sr_{0.5}Mn_{1-x}Co_xO_3$ was obtained by calcining the precursor at a heating rate of 3 °C min^{-1} from ambient temperature to 900 °C in air in a muffle furnace and then kept at 900 °C for 3 h.

3 Results and Discussion

3.1 Composition Analysis of the Precursor

0.0300 g precursor sample was dissolved in 10 mL 50 vol.% HCl solution, then diluted to 100.00 mL with deionized water. Lanthanum (La), strontium (Sr), and manganese (Mn) in the solution were determined by inductively coupled plasma atomic emission spectrometry (ICP-AES, Perkin Elmer Optima 5300 DV). The results showed that the La, Sr, and Mn mass percentages were 21.03, 13.26, and 16.64 %, respectively. In other words, molar ratio of La/Sr/Mn in the precursor is 0.5:0.5:1.00.

3.2 XRD Analyses of the Calcined Products

Figure 1 shows the XRD patterns of calcined samples from different calcination temperatures. A highly crystallized $La_{0.5}Sr_{0.5}Mn_{1-x}Co_xO_3$ ($0 \leq x \leq 0.3$) with a perovskite structure is obtained when the precursor is calcined at 900 °C in air for 3 h (Fig 1a–d). The Co^{3+}-doped ions do not obviously change the perovskite crystalline structure of ABO_3. As shown in the XRD patterns (Fig. 1e), a slight shift of the peaks of XRD to a higher angle is observed in the Co^{3+}-doped $La_{0.5}Sr_{0.5}Mn_{1-x}Co_xO_3$ due to the smaller ionic radii of Co^{3+} (0.061 nm) [31] than that of Mn^{3+} (0.064 nm) [32]. The refined lattice parameters of $La_{0.5}Sr_{0.5}Mn_{1-x}Co_xO_3$ ($x = 0$, 0.1, 0.2,

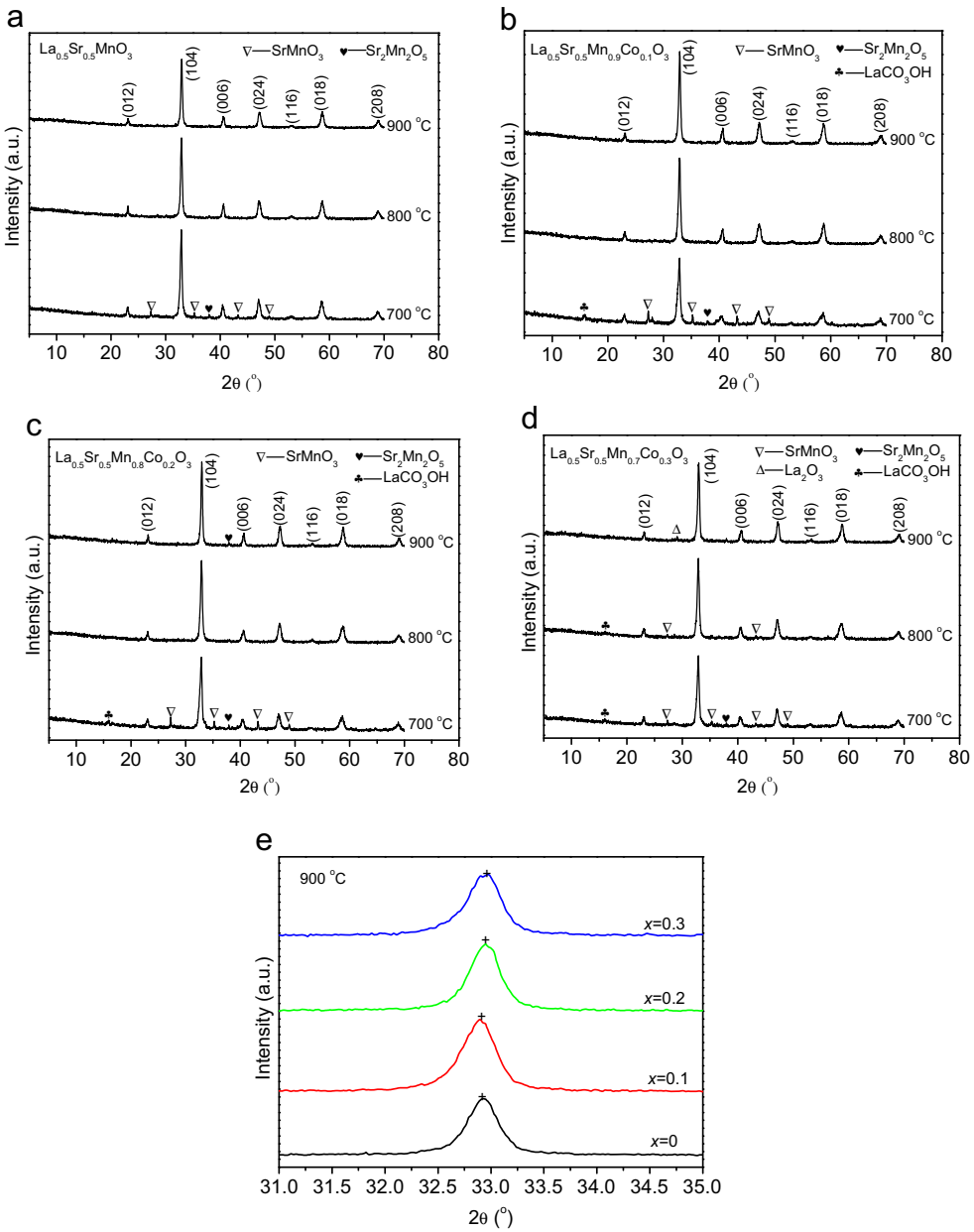

Fig. 1 **a–e** The XRD patterns of $La_{0.5}Sr_{0.5}Mn_{1-x}Co_xO_3$

and 0.3) calcined at 900 °C were obtained. The results are shown in Table 1. With the increase of doped Co^{3+} amount from $x = 0$, 0.1, 0.2 to 0.3, lattice parameters a and b values decrease but a slight increase for $x = 0.3$. This could be due to smaller Co^{3+} (0.061 nm) [31] ions substituting Mn^{3+} (0.064 nm) [32] initially, and then for higher doping level, some of Co^{3+} may substitute the Mn^{4+} (with much smaller ionic radius of 0.053 nm [33]). A similar phenomenon was also observed for $La_{0.5}Sr_{0.5}Mn_{1-x}Ti_xO_3$ [33].

Compared to solid-state reaction at high temperatures using a mixture of La_2O_3, $SrCO_3$, $MnCO_3$, and Co_2O_3 [27, 30], the crystallization temperature of $La_{0.5}Sr_{0.5}Mn_{1-x}Co_xO_3$ in this study is lower, while the crystallinity of $La_{0.5}Sr_{0.5}Mn_{1-x}Co_xO_3$ is higher. This finding is attributed to the fact that direct high-temperature solid-state reaction induces difficult penetration between solid particles, resulting in the crystallization

Table 1 The lattice parameter of $La_{0.5}Sr_{0.5}Mn_{1-x}Co_xO_3$ with $x = 0$, 0.1, 0.2, and 0.3

Co content	a (nm)	b (nm)	c (nm)
0.0	0.54468	0.54468	0.77580
0.1	0.54454	0.54454	0.77624
0.2	0.54363	0.54363	0.77685
0.3	0.54367	0.54367	0.77662

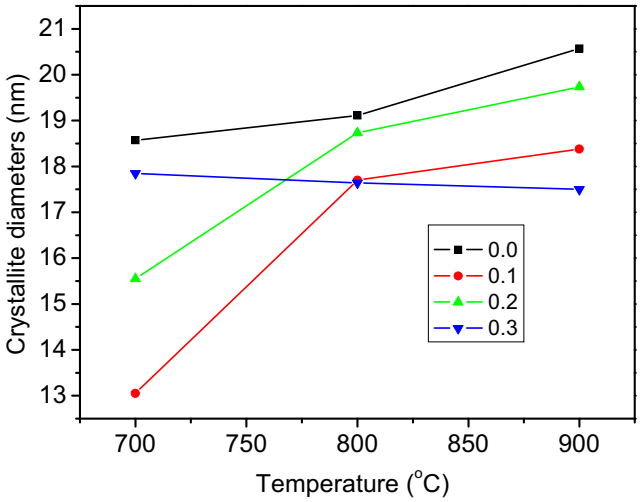

Fig. 2 The dependence of crystallite diameters of $La_{0.5}Sr_{0.5}Mn_{1-x}Co_xO_3$ on calcination temperature

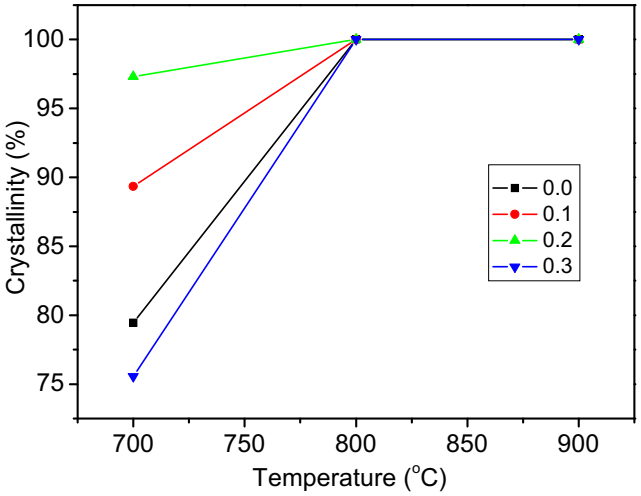

Fig. 4 The dependence of $La_{0.5}Sr_{0.5}Mn_{1-x}Co_xO_3$ crystallinity on calcination temperature

of $La_{0.5}Sr_{0.5}MnO_3$ and $La_{0.7}Sr_{0.3}Mn_{1-x}Co_xO_3$ at higher temperature. However, a mixture of $La(NO_3)_3{\cdot}6H_2O$, $SrCl_2$, $MnCl_2{\cdot}4H_2O$, $CoSO_4{\cdot}7H_2O$, and Na_2CO_3 was ground at room temperature in our study. Precursor carbonates can be obtained with molecular-level scale after uniform mixing. Single-phase crystalline $La_{0.5}Sr_{0.5}Mn_{1-x}Co_xO_3$ can then be obtained at a lower temperature when the precursor is calcined in air.

The crystallite diameter of $La_{0.5}Sr_{0.5}Mn_{1-x}Co_xO_3$ was estimated using the Scherrer formula [34]:

$$D = K\lambda/(\beta\cos\theta) \tag{1}$$

where D is the crystallite diameter, $K = 0.89$ (the Scherrer constant), $\lambda = 0.15406$ nm (wavelength of the X-ray used), β is the width of line at the half-maximum intensity, and θ is the corresponding angle. From the position of the (1 0 4) peak ($2\theta_{(1\,0\,4)}$) in XRD patterns, the $d_{(1\,0\,4)}$ interplanar spacing is determined using the Bragg equation [36]:

$$d_{(1\,0\,4)} = \frac{\lambda}{2\sin\theta_{(1\,0\,4)}} \tag{2}$$

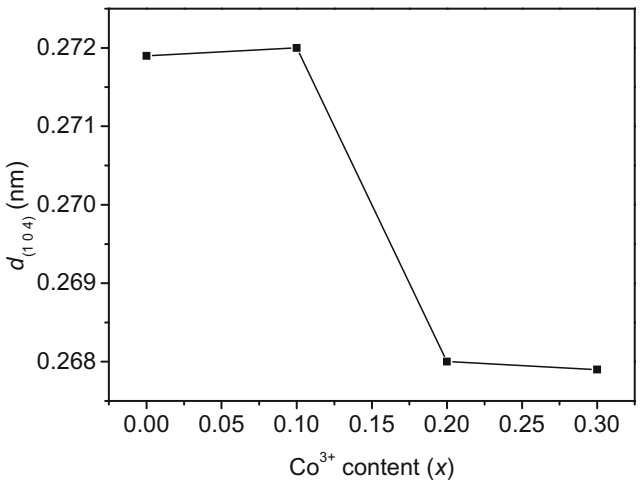

Fig. 3 The dependence of interplanar spacing ($d_{(1\,0\,4)}$) of $La_{0.5}Sr_{0.5}Mn_{1-x}Co_xO_3$ on Co^{3+} content

The crystallite diameter (D) of $La_{0.5}Sr_{0.5}Mn_{1-x}Co_xO_3$ from calcining the precursor at different temperatures and $d_{(1\,0\,4)}$ interplanar spacing of $La_{0.5}Sr_{0.5}Mn_{1-x}Co_xO_3$ obtained at 900 °C are shown in Figs. 2 and 3, respectively. From Fig. 2, it can be seen that after the addition of Co^{3+} ions, the average crystallite size of samples decreases slightly and reaches the lowest value (17.5 nm) when x is 0.3. The binding energy of Co^{3+}–O^{2-} is larger than that of Mn^{3+}–O^{2-}, attributed to the Co^{3+} ion (0.061 nm) having smaller radii than Mn^{3+} ion (0.064 nm). When Co^{3+} ions enter into the lattice to form the Co^{3+}–O^{2-} bonds, the crystal nucleation and growth of Co^{3+}substituted (La, Sr)MnO_3 manganite (LSMO) will consume more energy, which results in a smaller average crystallite diameter for substituted LSMO manganite. The $d_{(1\,0\,4)}$ values of the samples in Fig. 3 reveal that the interplanar spacing increases slightly with the addition of small amount of Co^{3+} ions which is consistent with the XRD result in Fig. 1e. It can be clearly seen from Fig. 2e that the (1 0 4) peak shifts slightly to higher degrees with the increase of Co^{3+} content. The increase in interplanar spacing of samples can be explained on the basis of the radii of metal ions. The radius of Co^{3+} ion (0.061 nm) is smaller than that of Mn^{3+} ion (0.064 nm). Therefore, the Co^{3+} ion could locate in the B sublattice with adequate space. The replacement of Mn^{3+} ions in $La_{0.5}Sr_{0.5}MnO_3$ by Co^{3+} ions could cause the contraction of the unit cell (such as a and b values), resulting in the decrease of interplanar spacing [37, 38].

The crystallinity of $La_{0.5}Sr_{0.5}Mn_{1-x}Co_xO_3$ can be calculated by MDI Jade 5.0 software. The crystallinity of

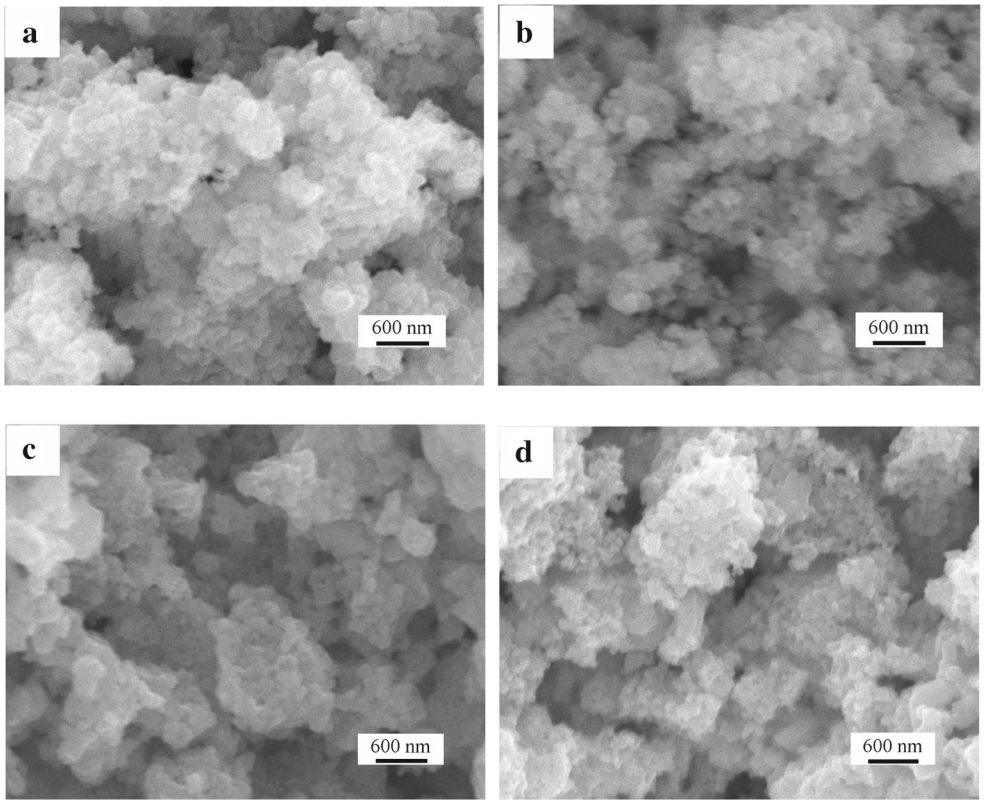

Fig. 5 SEM images of $La_{0.5}Sr_{0.5}Mn_{1-x}Co_xO_3$ synthesized at 900 °C in air for 3 h: **a** $La_{0.5}Sr_{0.5}MnO_3$, **b** $La_{0.5}Sr_{0.5}Mn_{0.9}Co_{0.1}O_3$, **c** $La_{0.5}Sr_{0.5}Mn_{0.8}Co_{0.2}O_3$, and **d** $La_{0.5}Sr_{0.5}Mn_{0.7}Co_{0.3}O_3$

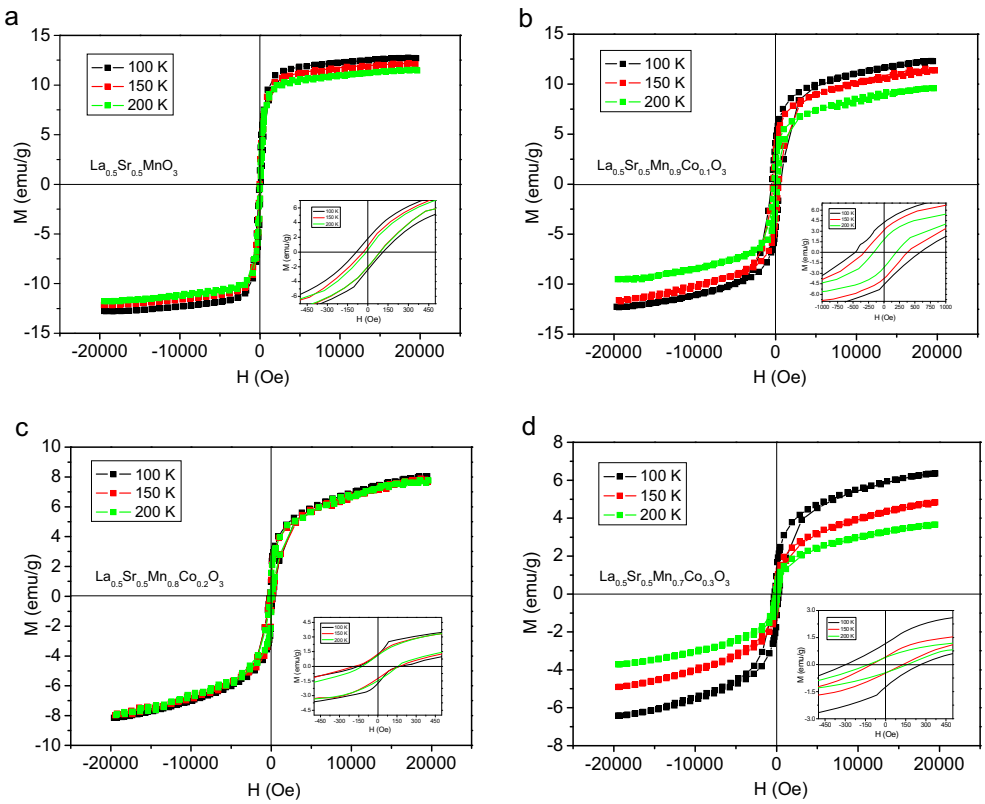

Fig. 6 **a**–**d** $M-H$ (magnetization–hysteresis) loops of $La_{0.5}Sr_{0.5}Mn_{1-x}Co_xO_3$ samples obtained at 900 °C and different measurement temperatures

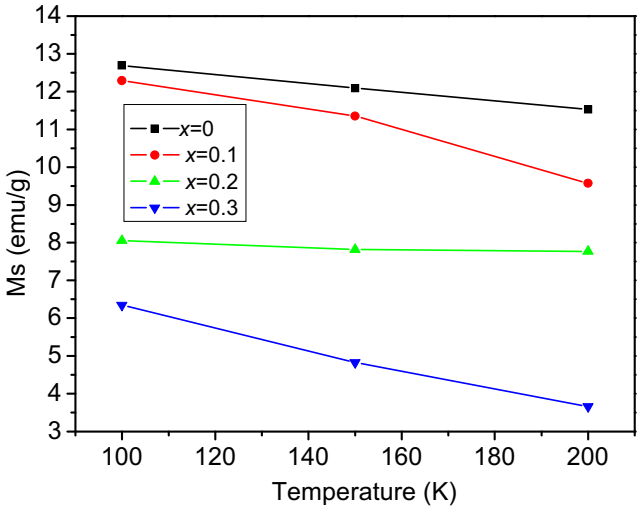

Fig. 7 The dependence of specific saturation magnetization of $La_{0.5}Sr_{0.5}Mn_{1-x}Co_xO_3$ on Co^{3+} content and measurement temperature

$La_{0.5}Sr_{0.5}Mn_{1-x}Co_xO_3$ ($x = 0$, 0.1, 0.2, and 0.3) obtained at different temperatures is shown in Fig. 4. The crystallinities of $La_{0.5}Sr_{0.5}Mn_{1-x}Co_xO_3$ ($x = 0$, 0.1, and 0.2) obtained at 700 °C increase with increasing Co^{2+} content except for $La_{0.5}Sr_{0.5}Mn_{0.7}Co_{0.3}O_3$. However, the crystallinity of $La_{0.5}Sr_{0.5}Mn_{1-x}Co_xO_3$ obtained above 800 °C is approximately 100 %.

Lattice strains of the $La_{0.5}Sr_{0.5}Mn_{1-x}Co_xO_3$ were estimated using the Williamson–Hall formula [39, 40]:

$$\varepsilon = \frac{B}{4\tan\theta} \tag{3}$$

where B is the full width at half of the maximum (in radian) of the peaks, θ is the peak position, and ε is the lattice strain of the structure. The lattice strains of $La_{0.5}Sr_{0.5}Mn_{1-x}Co_xO_3$ obtained at 900 °C are 0.598 % for $x = 0$, 0.636 % for $x = 0.1$, 0.552 % for $x = 0.2$, and 0.541 % for $x = 0.3$, respectively. That is, the lattice strain of $La_{0.5}Sr_{0.5}Mn_{1-x}Co_xO_3$ increases with the increase of Co^{3+} content and/or the decrease of Mn^{3+} content between $x = 0$ and $x = 0.1$ at first, then decreases with the increase of Co^{3+} content, which can be attributed to the Co^{3+} ion (0.061 nm) having a smaller radius than the Mn^{3+} ion (0.064 nm). The replacement of Mn^{3+} ions in $La_{0.5}Sr_{0.5}Mn_{1-x}Co_xO_3$ by Co^{3+} ions would cause the decrease of the unit cell (a and b values), resulting in the increase of lattice strain in $La_{0.5}Sr_{0.5}Mn_{1-x}Co_xO_3$. For higher doping level, some of Co^{3+} may substitute the Mn^{4+} (with much smaller ionic radius of 0.053 nm), which would cause the expansion of the unit cell (c value), resulting in the decrease of lattice strain in $La_{0.5}Sr_{0.5}Mn_{1-x}Co_xO_3$.

3.3 SEM Analyses of the Calcined Products

The morphologies of the calcined products are shown in Fig. 5. Figure 5a shows that the $La_{0.5}Sr_{0.5}MnO_3$ sample obtained at 900 °C is composed of approximately spherical grains and contains particles having a distribution from 80 to 250 nm. Figure 5b–d shows the SEM images of the $La_{0.5}Sr_{0.5}Mn_{1-x}Co_xO_3$ ($x = 0.1$, 0.2, and 0.3) samples obtained at 900 °C, respectively. The $La_{0.5}Sr_{0.5}Mn_{1-x}Co_xO_3$ ($x = 0.1$, 0.2, and 0.3) sample is also composed of approximately spherical grains. The particle sizes are mainly between 70 and 200 nm. The average crystallite sizes of the calcined samples determined by X-ray diffraction were significantly smaller than the values determined by SEM. This difference can be attributed to the fact that the values observed by SEM have the size of the secondary particles, which are composed of several or many crystallites by soft reunion. In addition, the X-ray line broadening analysis disclosed only the size of a single crystallite.

3.4 Magnetic Properties of $La_{0.5}Sr_{0.5}Mn_{1-x}Co_xO_3$

Hysteresis loops of $La_{0.5}Sr_{0.5}Mn_{1-x}Co_xO_3$ samples calcined at 900 °C at different measurement temperatures are shown in Fig. 6. Figure 7 shows the dependence of specific

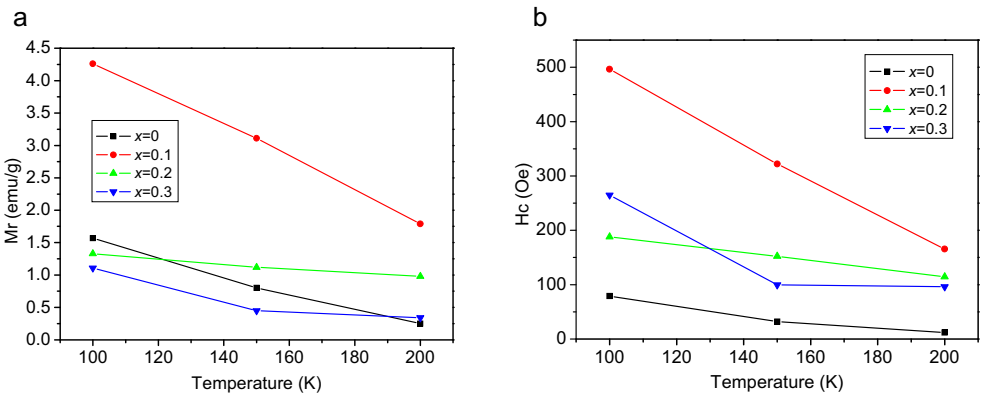

Fig. 8 **a–b** The dependence of remanence (M_r) and coercivity (H_c) of $La_{0.5}Sr_{0.5}Mn_{1-x}Co_xO_3$ on Co^{3+} content and measurement temperature

magnetization of $La_{0.5}Sr_{0.5}Mn_{1-x}Co_xO_3$ on doping Co^{3+} amount and measurement temperature. The specific magnetization decreases with the increase of Co^{3+} concentration in the sample and measurement temperature (see Fig. 7). It can be attributed to the substitution of Mn^{3+} (0.064 nm) and/or Mn^{4+} (0.053 nm) by Co^{3+} (0.061 nm) which promotes a cation arrangement in $La_{0.5}Sr_{0.5}Mn_{1-x}Co_xO_3$, resulting in the decrease of specific magnetization for $La_{0.5}Sr_{0.5}Mn_{1-x}Co_xO_3$. Among $La_{0.5}Sr_{0.5}Mn_{1-x}Co_xO_3$ ($x = 0$, 0.1, 0.2, and 0.3), $La_{0.5}Sr_{0.5}MnO_3$ at 100 K measurement temperatures has the highest specific magnetization value, 12.69 emu/g. The dependence of remanence (M_r) and coercivity (H_c) on Co^{3+} content is shown in Fig. 8. $La_{0.5}Sr_{0.5}Mn_{0.9}Co_{0.1}O_3$ at 100 K measurement temperatures has the highest remanence (4.26 emu/g) and coercivity (496.24 Oe).

The magnetic moment of $La_{0.5}Sr_{0.5}Mn_{1-x}Co_xO_3$ samples obtained at 900 °C was estimated using the following relationship [41, 42]:

$$\eta_B = M_w \times M/5585 \quad (4)$$

where M_w is the molecular weight of the composition, M is the specific magnetization (emu/g) at an applied field of 19.5 kOe, and η_B is the magnetic moment (Bohr magneton, B.M.). The magnetic moment values of $La_{0.5}Sr_{0.5}Mn_{1-x}Co_xO_3$ are shown in Fig. 9. The magnetic moment value of $La_{0.5}Sr_{0.5}Mn_{1-x}Co_xO_3$ at an applied field of 19.5 kOe decreases with the increase of Co^{3+} concentration in the sample and measurement temperature. $La_{0.5}Sr_{0.5}MnO_3$ at 100 K has the highest magnetic moment value (0.491 B.M.).

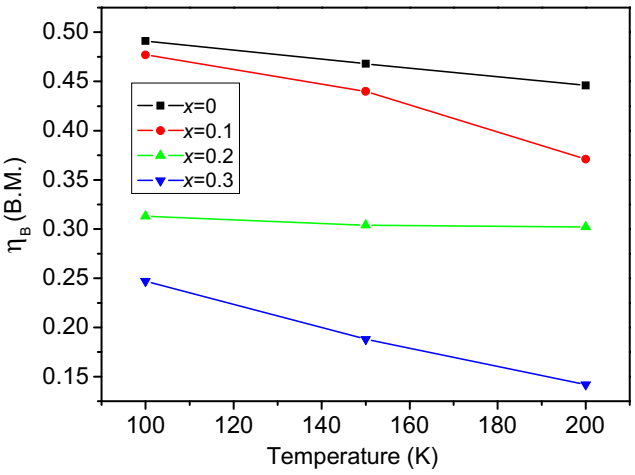

Fig. 9 The dependence of magnetic moment of $La_{0.5}Sr_{0.5}Mn_{1-x}Co_xO_3$ on Co^{3+} content and measurement temperature

4 Conclusions

$La_{0.5}Sr_{0.5}Mn_{1-x}Co_xO_3$ ($x = 0$, 0.1, 0.2, and 0.3) was successfully synthesized by calcining the precursor carbonates in air. The XRD analysis suggests that a rhombohedral $La_{0.5}Sr_{0.5}Mn_{1-x}Co_xO_3$ ($x = 0$, 0.1, 0.2, and 0.3) with space group Pnma (62) can be obtained by calcining the precursor over 800 °C in air for 3 h. Lattice parameters (a and b values) decrease with the increase of Co^{3+} additional amount but a slight increase for $x = 0.3$. Magnetic characterization indicates that the magnetic properties of $La_{0.5}Sr_{0.5}Mn_{1-x}Co_xO_3$ depend on the composition and measurement temperature. Substitution of Mn^{3+} and/or Mn^{4+} ion by Co^{3+} ion in $La_{0.5}Sr_{0.5}Mn_{1-x}Co_xO_3$ decreases specific magnetization. However, the coercivity of $La_{0.5}Sr_{0.5}Mn_{1-x}Co_xO_3$ can be markedly improved after doping Co^{3+} ion.

Acknowledgments This study was financially supported by the National Natural Science Foundation of China (Grant no. 21161002) and the Guangxi University Student Innovation Foundation of China (Grant no. 30).

References

1. Qin, L.Q., Wu, X.H., Wang, K.T., Wu, W.W., Zhou, K.W., Liao, S.: J. Supercond. Nov. Magn. **27**, 2751–2756 (2014)
2. Giri, S.K., Nath, T.K.: J. Supercond. Nov. Magn. **28**, 895–900 (2015)
3. Ho, T.A., Thanh, T.D., Phan, T.L., Oh, S.K., Yu, S.C.: J. Supercond. Nov. Magn. **28**, 891–894 (2015)
4. Sbissi, K., Kahn, M.L., Ellouze, M., Hlil, E.K., Elhalouani, F.: J. Supercond. Nov. Magn. **28**, 1433–1438 (2015)
5. Kolat, V.S., Esturk, U., Izgi, T., Gencer, H., Atalay, S.: J. Alloys Compd. **628**, 1–8 (2015)
6. Zouari, S., Nasri, A., Ellouze, M., Hlil, E.K., Elhalouani, F.: J. Supercond. Nov. Magn. **27**, 1473–1481 (2014)
7. Ran, R., Wu, X.D., Quan, C.Z., Weng, D.: Solid State Ionics **176**, 965–971 (2005)
8. Huang, X.Q., Pei, L., Liu, Z.G., Lu, Z., Sui, Y., Qian, Z.N., Su, W.H.: J. Alloys Compd. **345**, 265–270 (2002)
9. Khlifi, M., Dhahri, E., Hlil, E.K.: J. Supercond. Nov. Magn. **27**, 1341–1345 (2014)
10. Yensano, R., Pinitsoontorn, S., Amornkitbamrung, V., Maensiri, S.: J. Supercond. Nov. Magn. **27**, 1553–1560 (2014)
11. Ma, J., Cai, Y.Q., Wang, W.Z., Cui, Q., Theingi, M., Zhang, H., Chen, Q.M.: Ceram. Int. **40**, 4963–4968 (2014)
12. Sarıboğa, V., Özdemir, H., Faruk Öksüzömer, M.A.: J. Eur. Ceram. Soc. **33**, 1435–1446 (2013)
13. Phillipps, M.B., Sammes, N.M., Yamamoto, O.: J. Mater. Sci. **31**, 1689–1692 (1996)
14. Jiang, S.P., Liu, L., Ong, K.P., Wu, P., Li, J., Pu, J.: J. Power Sources **176**, 82–89 (2008)
15. Morin, F., Trudel, G., Denos, Y.: Solid State Ionics **96**, 129–139 (1997)
16. Liu, X., Cheng, B., Hu, J.F., Qin, H.W., Jiang, M.H.: Sens. Actuators B **129**, 53–58 (2008)
17. Kruidhof, H., Bouwmeester, H.J.M., Doorn, R.H.Ev., Burggraaf, A.J.: Solid State Ionics **63–65**, 816–822 (1993)

18. Wei, Y.Y., Liu, H.F., Xue, J., Li, Z., Wang, H.H.: AIChE. J. **57**, 975–984 (2011)
19. Weidenkaff, A., Robert, R., Aguirre, M., Bocher, L., Lippert, T., Canulescu, S.: Renew. Energy **33**, 342–347 (2008)
20. Fu, S.S., Niu, H.L., Tao, Z.Y., Song, J.M., Mao, C.J., Zhang, S.Y., Chen, C.L., Wang, D.: J. Alloys Compd. **576**, 5–12 (2013)
21. Gaillard, F., Li, X.G., Uray, M., Vernoux, P.: Catal. Lett. **96**, 177–183 (2004)
22. Shimazaki, T., Yamazaki, T., Terayama, K., Yoshimura, M. J. Mater. Sci. Lett **19**, 2029–2031 (2000)
23. Zhang, X.X., Tejada, J., Xin, Y., Sun, G.F., Wong, K.W., Bohigas, X.: Appl. Phys. Lett. **69**, 3596–3598 (1996)
24. Guo, Z.B., Du, Y.W., Zhu, J.S., Huang, H., Ding, W.P., Feng, D.: Phys. Rev. Lett. **78**, 1142–1145 (1997)
25. Szewczyk, A., Szymczak, H., Wiśniewski, A., Piotrowski, K., Kartaszyński, R., Dabrowski, B., Koleśnik, S., Bukowski, Z.: Appl. Phys. Lett. **77**, 1026–1028 (2000)
26. Teng, F., Han, W., Liang, S.H., Gaugeu, B., Zong, R.L., Zhu, Y.F.: J. Catal. **250**, 1–11 (2007)
27. Shi, L., Yang, H.P., Zhou, S.M., Zhao, J.Y., He, L.F., Zhao, S.Y., Guo, Y.Q., Chen, L.: Solid State Commun. **150**, 371–374 (2010)
28. Shang, C., Xia, Z.C., Wei, M., Chen, B.R., Jin, Z., Huang, J.W., Shi, L.R., Ouyang, Z.W., Huang, S. Ceram. Int. **41**, 9708–9714 (2015)
29. Taran, S., Sun, C.P., Huang, C.L., Yang, H.D., Nigam, A.K., Chaudhuri, B.K., Chatterjee, S.: J. Alloys Compd. **644**, 363–370 (2015)
30. Phan, T.L., Thanh, T.D., Yu, S.C.: J. Alloys Compd. **615**, S247—S251 (2014)
31. Amer, M.A., Meaz, T.M., Mostafa, A.G., El-Kastawi, M., Ghoneim, A.I.: Ceram Int. **40**, 241–248 (2014)
32. Güner, S., Amir, M., Geleri, M., Sertkol, M., Baykal, A.: Ceram Int. doi:10.1016/j.ceramint.2015.05.034
33. Shang, C., Xia, Z.C., Jin, Z., Shi, L.R., Huang, J.W., Chen, B.R., Wei, M., Xiao, L.X., Liu, L., Huang, Y.: J Alloys Compd. **588**, 53–58 (2014)
34. Wu, W.W., Cai, J.C., Wu, X.H., Liao, S., Wang, K.T., Tao, L.: Adv Powder Technol. **24**, 154–159 (2013)
35. Zhou, K.W., Wu, X.H., Wu, W.W., Xie, J., Tang, S.Q., Liao, S.: Adv Powder Technol. **24**, 359–363 (2013)
36. Li, D.Y., Sun, Y.K., Xu, Y., Ge, H.L., Wu, Q., Yan, C.: Ceram. Int. **41**, 4581–4589 (2015)
37. Ateia, E.E., Ahmed, M.A., Salah, L.M., El-Gamal, A.A.: Physica B: Condens. Matter **445**, 60–67 (2014)
38. Peng, Z.J., Fu, X.L., Ge, H.L., Fu, Z.Q., Wang, C.B., Qi, L.H., Miao, H.Z.: J. Magn. Magn. Mater. **323**, 2513–2518 (2011)
39. Williamson, G.K., Hall, W.H.: Acta Metall. **1**, 22–31 (1953)
40. Chen, W., Wu, W.W., Liu, S.Q., Xu, J.W., Liu, D.S., Wu, X.H., Zhou, Y., Wu, J.: Mater. Sci. Semicond. Process **39**, 544–550 (2015)
41. Venkata Reddy, C., Byon, C., Narendra, B., Baskar, D., Srinivas, G., Shim, J., Prabhakar Vattikuti, S.V.: Superlattices Microstruct. **82**, 165–173 (2015)
42. Mane, D.R., Birajdar, D.D., Shirsath, S.E., Telugu, R.A., Kadam, R.H.: Phys. Status Solidi A **207**, 2355–2363 (2010)